

PAPER • OPEN ACCESS

Following O and OH in He/O₂ and He/H₂O gas mixtures—from the gas phase through the liquid phase to modifications on a biological sample

To cite this article: Katharina Stapelmann *et al* 2021 *J. Phys. D: Appl. Phys.* **54** 434003

View the [article online](#) for updates and enhancements.

You may also like

- [Effect of N₂ and O₂ on OH radical production in an atmospheric helium microwave plasma jet](#)
Nimisha SRIVASTAVA and Chuji WANG
- [The effects of radio frequency atmospheric pressure plasma and thermal treatment on the hydrogenation of TiO₂ thin film](#)
Yu ZHANG, , Haozhe WANG *et al.*
- [HCOO_{aq} degradation in droplets by OH_{aq} in an atmospheric pressure glow discharge](#)
Mackenzie Meyer, Gaurav Nayak, Peter J Bruggeman *et al.*



ECS
The
Electrochemical
Society
Advancing solid state &
electrochemical science & technology

DISCOVER
how sustainability
intersects with
electrochemistry & solid
state science research

Following O and OH in He/O₂ and He/H₂O gas mixtures—from the gas phase through the liquid phase to modifications on a biological sample

Katharina Stapelmann* , Brayden Myers, Maria Herrera Quesada , Eleanor Lenker and Pietro J Ranieri 

Department of Nuclear Engineering, North Carolina State University, Raleigh, NC, United States of America

E-mail: kstapel@ncsu.edu

Received 16 May 2021, revised 28 June 2021

Accepted for publication 29 July 2021

Published 9 August 2021



CrossMark

Abstract

Applied cold atmospheric plasma allows for the controlled delivery of reactive oxygen and nitrogen species tailored for specific applications. Through the manipulation of the plasma parameters, feed gases, and careful consideration of the environment surrounding the treatment target, selective chemistries that preferentially influence the target can be produced and delivered. To demonstrate this, the COST reference microscale atmospheric pressure plasma jet is used to study the generation and transport of O and ·OH from the gas phase through the liquid to the biological model target cysteine. Relative and absolute species densities of ·OH and O are measured in the gas phase through laser induced fluorescence (LIF) and two-photon absorption LIF respectively. The transport of these species is followed into the liquid phase by hydrogen peroxide quantification and visualized by a fluorescence assay. Modifications to the model biological sample cysteine exposed to ·OH and H₂O₂ dominated chemistry (He/H₂O (0.25%)) and O dominated chemistry (He/O₂ (0.6%)) is measured by FTIR spectroscopy. The origin of these species that modify cysteine is considered through the use of heavy water (H₂¹⁸O) and mass spectrometry. It is found that the reaction pathways differ significantly for He/O₂ and He/H₂O. Hydrogen peroxide is formed mainly in the liquid phase in the presence of a substrate for He/O₂ whereas for He/H₂O it forms in the gas phase. The liquid chemistry resulting from the He/O₂ admixture mainly targets the sulfur moiety of cysteine for oxidation up to irreversible oxidation states, while He/H₂O treatment leads preferentially to reversible oxidation products. The more O or OH/H₂O₂ dominated chemistry produced by the two gas admixtures studied offers the possibility to select species for target modification.

* Author to whom any correspondence should be addressed.



Original Content from this work may be used under the terms of the [Creative Commons Attribution 4.0 licence](https://creativecommons.org/licenses/by/4.0/). Any further distribution of this work must maintain attribution to the author(s) and the title of the work, journal citation and DOI.

Keywords: plasma diagnostics, plasma liquid interactions, plasma biology, LIF, FTIR, mass spectrometry

(Some figures may appear in colour only in the online journal)

1. Introduction

Atmospheric pressure plasma jets (APPJs) are a source of a variety of reactive species which can be delivered to various targets, e.g. water for plasma agriculture applications or biological targets for plasma medicine. In both applications, reactive oxygen and reactive nitrogen species (RONS) play a key role. Thus, the controlled delivery of RONS from the plasma to the target is one of the key challenges for plasma agriculture and plasma medicine. Biological targets are typically surrounded by a liquid environment, which offers another layer of complexity for following the generation and transport of reactive species. In particular, reactive oxygen species (ROS) like atomic oxygen O or the hydroxyl radical $\cdot\text{OH}$ are of interest as they are highly reactive and have been shown to cause major modifications on different organic targets, e.g. cancer cells [1, 2], proteins and amino acids [3–7], and phenol [8, 9]. To produce O or $\cdot\text{OH}$ inside an APPJ, a noble gas like helium or argon is typically used with some admixtures, e.g. O_2 or water vapor. Reactive species can be produced inside the APPJ, either due to the process gas used or due to impurities, or in the effluent when high-energetic and/or reactive species interact with ambient air. Reactive species produced in the gas phase can then undergo further reactions in the gas phase before approaching the liquid interface. In case of atomic oxygen, the main loss reaction is the formation of ozone by the three-body reaction $\text{O} + \text{O}_2 + \text{M} \rightarrow \text{O}_3 + \text{M}$. The major loss mechanism of OH is the recombination to hydrogen peroxide in the gas phase [10]. Once O and OH have entered the liquid, further reactions occur in the liquid phase. If a biological target is present, the target itself becomes part of the reaction pathway.

The plethora of APPJ's developed in different laboratories makes it difficult to compare results and to gain fundamental understanding of the generation and transport of the species produced. To overcome this, the COST radio frequency (RF) plasma jet was developed in the frame of an EU COST action as a reference APPJ, introduced and described in detail in Golda *et al* [11]. The production of species by the COST-jet and similar devices has been studied in the gas phase using, e.g. optical emission spectroscopy [12], molecular beam mass spectrometry [13–15], two-photon absorption laser-induced fluorescence (TALIF) [15–18], and cavity ring-down laser absorption spectroscopy [15]. Further investigations have been performed in the liquid phase with electron paramagnetic resonance (EPR) spectroscopy, ion chromatography, and colorimetric assays [6, 19, 20]. These studies lay a framework for detailing the initial plasma parameters to deliver specific reactive species from the plasma to the target and help contextualize the results presented here.

We will follow the generation and transport of O and $\cdot\text{OH}$ from the gas phase in the presence of a liquid target, through the liquid to the model biological substrate cysteine. Fourier transform infrared (FTIR) spectroscopy of cysteine has previously been introduced as a ready-to-use method for the investigation of plasma-induced modifications [21] and has been used to compare chemical modifications caused by different plasma sources and gas admixtures [3, 6, 22]. The amino acid cysteine is a simple model, containing each chemical group only once which allows identifying chemical modifications easily. Its amino ($\text{R}-\text{NH}_2$), carboxyl ($\text{R}-\text{COOH}$) and thiol ($\text{R}-\text{SH}$) groups can be found in almost every biologically relevant macromolecule. Especially the thiol group is of biological relevance as the importance of thiol modifications has been recognized in redox biology [23–26]. We compare the modifications on cysteine exposed to $\cdot\text{OH}$ and H_2O_2 dominated chemistry and an O dominated chemistry in the liquid. Further, we link the chemical modifications observed with liquid phase and gas phase chemistry, in the presence of a liquid interface.

The paper is organized as follows: first, the experimental set-up and the diagnostic set-ups for the gas phase, the liquid phase, and the biological samples are briefly described. The results section is split in four parts: first, the gas phase results obtained by laser induced fluorescence (LIF) and two-photon absorption laser induced fluorescence (TALIF) are presented; in the next part, the transport of atomic oxygen and OH is discussed with liquid phase measurements in correlation to the gas phase measurements. In the third part, the transport of the species to a biological target is explored by investigating modifications occurring on the model biological sample cysteine by means of FTIR spectroscopy and mass spectrometry. The origin of the reactive species responsible for the chemical modifications is explored by using heavy water (H_2^{18}O) for the cysteine solution. Finally, conclusions are drawn.

2. Experimental setup

2.1. Plasma source

The plasma source used for the experiments is the atmospheric pressure COST reference microplasma jet, described in more detail in Golda *et al* [11]. Briefly, the COST-jet is a capacitively coupled RF plasma, driven at a frequency of 13.56 MHz. The electrodes are 30 mm long and 1 mm apart from each other, resulting in an active plasma region of $1 \text{ mm} \times 1 \text{ mm} \times 30 \text{ mm}$. Helium is used as the feed gas with small admixtures of either oxygen (0.6%) or water (0.25% equivalent to 2500 ppm). The gas flow is kept constant at 1 slm for all experiments. Helium and oxygen (ARC3, 5.0 purity) is delivered via stainless steel tubing to reduce impurities. For

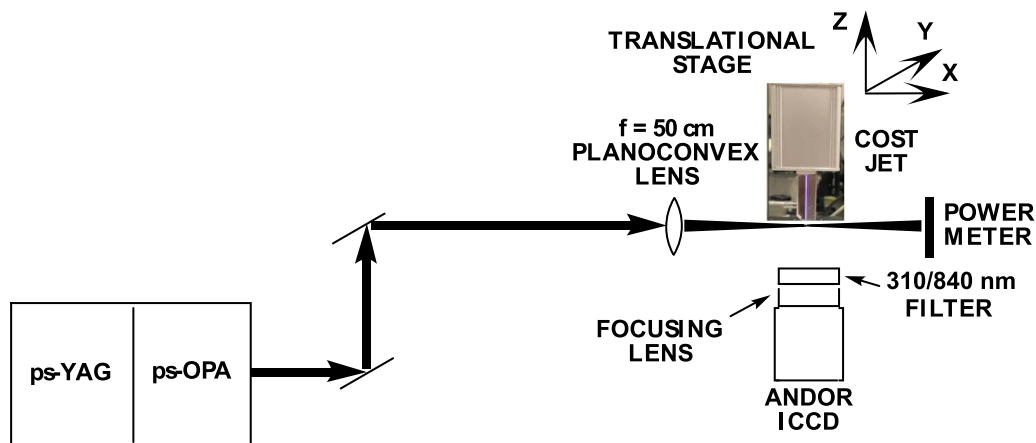


Figure 1. Laser setup for OH LIF and O TALIF measurements.

the He/H₂O mixture, dry helium is passed through a bubbler and mixed back with dry helium downstream in the appropriate ratio. Power is kept constant at 750 ± 10 mW and continuously monitored by integrated current and voltage probes.

2.2. Gas phase diagnostics

Atomic oxygen and OH were measured in the effluent with and without a liquid target present. Atomic oxygen densities in the effluent were measured using two-photon absorption laser induced fluorescence (TALIF) [27] and OH was determined using laser induced fluorescence (LIF). For the measurements with a liquid surface present, a cylinder with a volume of 60 ml is filled with DI water and placed at a 4 mm distance to the jet's nozzle. The experimental setup is depicted in figure 1.

2.2.1. TALIF for atomic oxygen. Details of the TALIF setup and the density calibration can be found in Myers *et al* [27]. Briefly, a Nd:YAG laser (EKSPILA) with a 30 ps pulse width and a 50 Hz repetition frequency was used to produce 10 μ J pulse energies. The TALIF signal is recorded with an Andor ISTAR Gen III intensified CCD camera. The ICCD camera is used in conjunction with an 840 nm filter (Andover Corporation, FWHM 10 nm). For spatial scans of the effluent, the laser and detector setup is fixed, while the plasma jet and liquid surface are moved on an $x - y - z$ translational stage. Densities of atomic oxygen found using absolutely-calibrated TALIF are estimated to have an experimental uncertainty of 37% [27].

2.2.2. LIF for hydroxyl radicals. Laser induced fluorescence (LIF) of \cdot OH relies on exciting the ground state of the molecule using 283 nm photons tuned to the $\text{OH}(X^2\Pi(\nu = 0)) \rightarrow A^2\Sigma^+(\nu = 1)$ transition. From the $\text{OH}(A^2\Sigma^+(\nu = 1))$ excited state one of two processes can occur to produce emission in the wavelength region of interest, as shown in figure 2. The molecule can either de-excite to the $\text{OH}(X^2\Pi(\nu = 1))$ state, emitting a 315 nm photon, or undergo a vibrational energy transfer (VET) to the $\text{OH}(A^2\Sigma^+(\nu = 0))$ state, subsequently transitioning to the ground state and emitting a 309 nm photon.

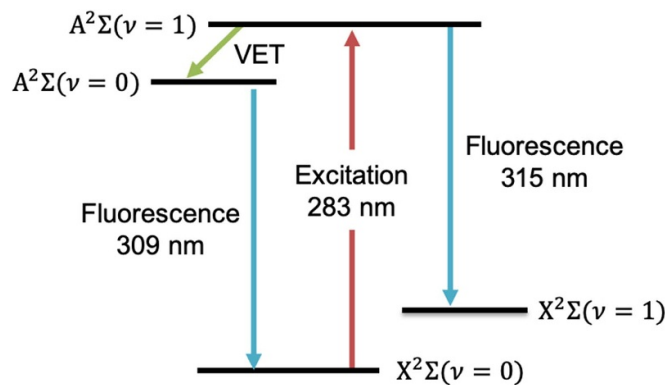


Figure 2. Excitation and fluorescence scheme for hydroxyl radicals. (VET = vibrational energy transfer.)

Alternatively, the laser-excited OH radical can be collisionally quenched, resulting in no emission. Due to the relatively long radiative lifetime of $\text{OH}(A^2\Sigma^+(\nu = 1))$ (more than 20 times longer than laser-excited O in TALIF measurements), collisional quenching is the dominant de-excitation pathway of the excited state [28, 29]. While helium does not collisionally quench laser-excited OH, the molecular components of the admixtures do so efficiently [30]. As a first-order approximation, the collisional quenching coefficients of H₂O and O₂ with $\text{OH}(A^2\Sigma^+(\nu = 1))$ were multiplied by the density of their respective admixtures (0.25% and 0.6%), and used for calculating the emission probability at all points in the effluent. Additionally, helium does not produce VETs in laser-excited OH; hence, the VET rate coefficients were applied in the same way for the two admixtures. After accounting for collisional quenching and VETs [31, 32], the resulting emission probabilities of $\text{OH}(A^2\Sigma^+(\nu = 1))$ in the He/H₂O effluent are 0.0214 for 315 nm emission and 0.0034 for 309 nm. For the He/O₂ admixture, emission probabilities of 0.0423 at 315 nm and 0.0101 at 309 nm were calculated. Two-dimensional spatial mapping of the OH LIF signal was plotted in Matlab (Mathworks).

Laser induced fluorescence (LIF) measurements of hydroxyl radicals in the effluent of the COST-jet were performed using the same laser as the TALIF measurements, an EKSPLA PL2230 Nd:YAG laser. A slightly lower pulse energy of 9 μJ was used for LIF. A linear relationship between laser power and fluorescence signal, indicative of no interference from laser-induced particle generation, was verified for pulse energies up to 12 μJ . The laser fluorescence was collected using an Andor iStar Gen III ICCD with an A-3 cathode, giving quantum efficiencies of approximately 10% for both fluorescence wavelengths. The ICCD was used along with a 310 nm filter (Andover Corporation, FWHM 10 nm), providing transmittance values of 0.152 at 309 nm and 0.124 at 315 nm. A gate width of 100 ns was used for all LIF measurements, while the acquisition time was varied between the two admixtures to maintain similar intensities of the raw LIF signal on the ICCD. Experimental uncertainty for LIF measurements was estimated to be 30%, owing primarily to the uncertainty in the applicability of collisional quenching rates in the effluent [27]. Variability in the fluorescence signal was considerably lower, generally less than 10% between measurements.

2.3. Liquid diagnostics

2.3.1. Hydrogen peroxide quantification. A xylenol orange based assay (PierceTM Quantitative Peroxide Assay Kit 23 280, Thermo Scientific) was used to detect hydrogen peroxide in 1 ml plasma-treated HPLC grade water, with and without 100 $\mu\text{g ml}^{-1}$ cysteine present in the solution. Solutions were treated in 12-well plates with the jet nozzle placed 4 mm from the surface of the liquid. Mock treatments were performed by adding hydrogen peroxide (Fisher Scientific, 30% stock solution (v/v) at 8.8 M) in concentrations equivalent to the investigated treatment times to the cysteine solution to determine the consumption of hydrogen peroxide by cysteine. Samples were diluted depending on treatment and left to incubate, with 400 μl of working reagent mixture at room temperature, for 20 min. The absorbance of the dye was detected photometrically at 560 nm through the use of a deuterium-halogen lamp (Ocean Optics DH-2000-BAL) and the Ocean Optics QE Pro spectrometer. Average and standard deviation are plotted in Origin (OriginLab).

2.3.2. pH Measurements. pH was monitored for each treatment condition. The cysteine solutions, for both gas admixtures, at 0 min (control), 0.5 min, 1 min, and 5 min had corresponding pH values of 5.5, 4.5, 4.1, and 3.5, respectively. All measurements were taken in triplicate with a pH probe (Hanna Instruments Laboratory Research Grade Benchtop pH/mV/ISE Meter, HI5522-01, probe HI1083B) and have a standard deviation of less than 0.16.

2.3.3. Visualization of atomic O in liquid. The terephthalic acid (TA, 99+%, Acros Organics) assay was used to visualize the transport of species in the liquid. TA is supposed to react selectively with OH to form HTA, which is fluorescent at 425 nm. Although we previously found the TA assay not to be selective in the presence of atomic oxygen [19], the assay is used here only to visualize the transport of the HTA product in the liquid when treated with atomic oxygen-dominated chemistry. Cuvettes were filled, all the way to the top, with 50 mM TA solution and placed at 1 mm gap distance from the COST-jet. Pictures of a He/O₂ plasma treatment were taken in a dark room with a Canon-EOS 6D digital camera (DSLR, 24–105 mm lens) while the cuvette was exposed to 310 nm light coming from a broadband laser-driven light source (Energetiq EQ-99XFC), located at 90° from the camera, and collimated through a fisheye lens. Resulting pictures were cropped and enhanced at 100% sharpness, 25% brightness, and 40% contrast.

2.4. Diagnostics on biological samples

The amino acid cysteine is used as a model biological sample. Here, we use FTIR spectroscopy and mass spectrometry to investigate the chemical modifications occurring on cysteine after plasma treatment.

2.4.1. Sample treatment. L-cysteine was obtained from Alfa Aesar (L-Cysteine A10435, $\geq 98\%$). Cysteine was dissolved in either HPLC grade water or heavy water (H₂¹⁸O, Medical Isotopes O2006, 97%) for a final concentration of 100 $\mu\text{g ml}^{-1}$. One milliliter of the solutions were transferred into 12-well plates and treated with the COST-jet at 4 mm distance. For both gas admixtures used, gas controls were taken where the cysteine solution was exposed to the respective gas flow for 5 min without igniting the plasma. All samples were treated in triplicate.

2.4.2. Fourier transform infrared spectroscopy. Dried samples were analyzed by FTIR spectroscopy. Aliquots of 20 μl were removed from each 1 ml sample and desiccated for 48 h on transmission FTIR silicon wafers prior to analysis. Spectra were obtained using the LUMOS FTIR microscope (Bruker) and recorded with a spectral resolution of 4 cm^{-1} with 64 scans per measurement. The spectra were baseline corrected by the rubberband correction method, and normalized through the vector normalization method in the Bruker OPUS software (Bruker Optic GmbH). Background spectra were taken for each silicon wafer before data collection. The experiments were performed in triplicates and for each sample, ten spectra were recorded at different positions and averaged. Standard deviation was calculated and is plotted as shadows Matlab.

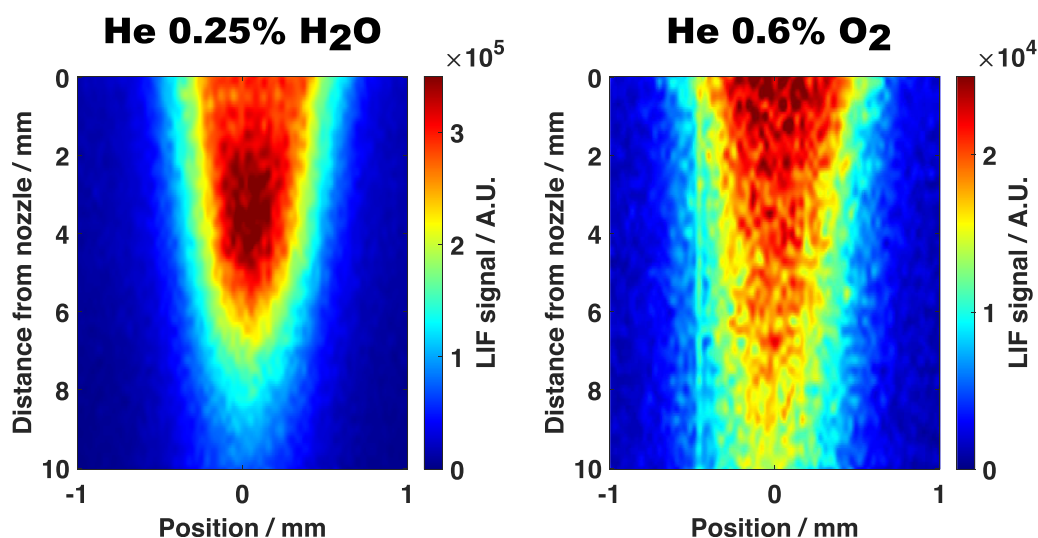


Figure 3. OH LIF signal in He/H₂O and He/O₂ plasma effluents out to 10 mm.

2.4.3. Mass spectrometry. 100 μL of each 1 ml sample was transferred to an autosampler vial for analysis by UPLC-MS/MS. The analysis was performed using a Thermo Vanquish LC instrument (Thermo Fisher Scientific, San Jose, CA) coupled to a Thermo Orbitrap Exploris 480 mass spectrometer (Thermo Fisher Scientific) with a heated electrospray ionization (HESI) source. Chromatographic separation was achieved on a Waters BEH Amide column (2.1 \times 100 mm, 1.8 μM) maintained at 45 $^{\circ}\text{C}$. The following linear gradient of mobile phase A (H₂O + 0.1% FA) and mobile phase B (MeCN + 0.1% FA) was used: 0–0.1 min (99% B, 0.4 ml min⁻¹), 0.1–7 min (99–30% B, 0.4 ml min⁻¹), 7–10 min (99% B, 0.4 ml min⁻¹). Samples were analyzed (2 μL injections) in positive ion mode (spray voltage 3.5 kV, ion transfer tube temperature 300 $^{\circ}\text{C}$, vaporizer temperature 350 $^{\circ}\text{C}$, sheath gas 50 a.u., aux gas 10 a.u., sweep gas 1 a.u.) with a mass range of m/z 60–1000. MS1 data was collected with a resolving power of 60 000 and an AGC target of 1×10^{-6} . MS2 data was collected with a resolving power of 30 000, cycle time of 0.6 s, and stepped HCD collision energy (30, 50, 150).

Raw data files were imported into Skyline [33] for peak picking and integration using a targeted data processing. Peak areas per sample for each target compound were exported from Skyline for figure generation in Origin.

3. Results

3.1. Generation of atomic oxygen and the hydroxyl radical in the gas phase in the presence of a liquid interface

Spatially resolved distributions of $\cdot\text{OH}$ were recorded in the effluent of the COST-jet using LIF for He/O₂ and He/H₂O admixtures in both an open effluent and in the presence of a water surface. The gap distance was set to 4 mm from the nozzle of the jet to the liquid interface, corresponding to previous liquid phase measurements [19]. In conjunction with absolutely-calibrated TALIF measurements of atomic oxygen

under identical conditions [27], a fairly complete picture of the progression of $\cdot\text{OH}$ and O in the effluent can be attained.

LIF measurements of $\cdot\text{OH}$ radicals, calibrated for the differing rates of collisional quenching and VETs of laser-excited $\cdot\text{OH}$ between admixtures, are shown in figure 3 for an unobstructed effluent. Unsurprisingly, the fluorescence signal was more than an order of magnitude higher for the He/H₂O admixture than its He/O₂ counterpart. This is a result of the much higher water concentration in the gas flow (water is only present as an impurity in the He/O₂ case), as H₂O dissociation in the active plasma is the dominant formation mechanism of $\cdot\text{OH}$ [34]. In addition to the relative fluorescence signal, the spatial distribution of $\cdot\text{OH}$ in the effluent is similar to that observed for O in previous work [27]. However, without measurements of the decay rates of laser-excited OH(A² Σ^+), it is difficult to make definitive statements about the evolution of $\cdot\text{OH}$ densities throughout the effluent. The fluorescence signal appears to increase out to a few mm in the He/H₂O effluent—a trend also observed for O in the He/H₂O case. Nonetheless, this is likely not a reflection of the $\cdot\text{OH}$ density distribution but rather the result of differences in the decay rates between the two positions. This assertion is supported by density measurements of $\cdot\text{OH}$ radicals in a similar APPJ at comparable water admixtures. Benedikt *et al* used two independent diagnostic techniques, cavity ring-down spectroscopy (CRDS) and molecular beam mass spectrometry (MBMS), which showed no increase in density with increasing distance from the nozzle [15]. Similar to atomic oxygen, the decay rate of laser-excited $\cdot\text{OH}$ is very sensitive to the background gas composition and a variety of species may contribute to a higher quenching rate close to the nozzle resulting in the lower apparent signal there. A second factor may be the temperature dependence of the collisional quenching of OH(A² Σ^+). The gas temperature across the effluent is relatively uniform but highest (around 330 K) at the nozzle before slowly thermalizing towards the effluent edge. Experiments have shown a $T^{0.5}$ relationship between the background gas temperature and quenching rate of laser-excited $\cdot\text{OH}$, affecting

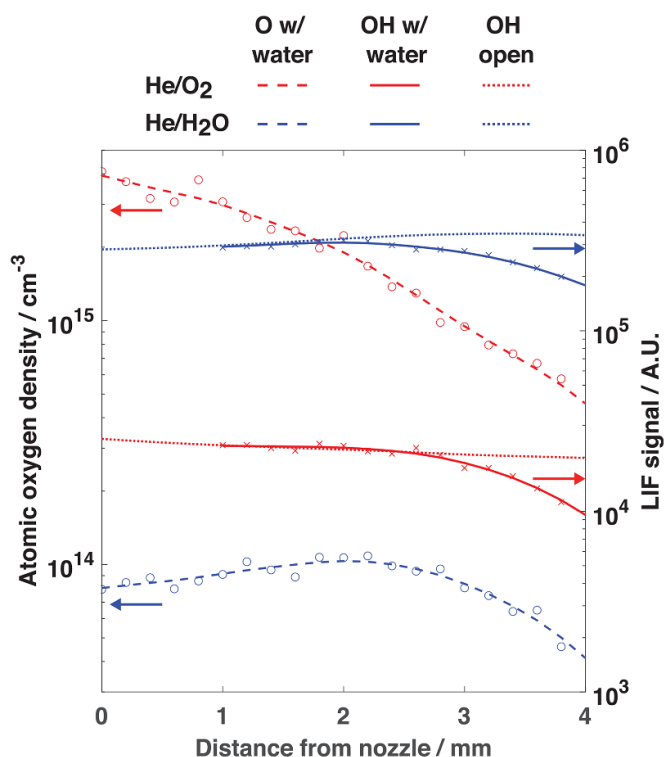


Figure 4. OH LIF signal in He/O₂ (red) and He/H₂O (blue) plasma effluents with a water surface present at 4 mm. Atomic O density detected through TALIF is overlaid for comparison. Reproduced from [27]. © IOP Publishing Ltd. CC BY 3.0.

both the $\nu = 1$ and $\nu = 0$ vibrational states [31, 35]. As a result, the elevated gas temperature close to the nozzle likely reduces the LIF signal in this region via increased collisional quenching.

The LIF measurements were repeated in the presence of a liquid surface at 4 mm. Figure 4 shows the relative LIF signal along the axis of the effluent plotted with the atomic oxygen densities [27] under the same conditions. Interestingly, the precipitous decline in the LIF signal observed near the water surface mirrors the density trend recorded for atomic oxygen. Although the LIF measurements cannot discern differences in quenching rates, determinations of the decay rates of laser-excited atomic oxygen indicate the background gas composition remains unchanged from the open effluent case for both admixtures [27]. This implies that the decrease in LIF signal corresponds to a lower $\cdot\text{OH}$ density rather than an artifact of faster decay rates in this region. Furthermore, the similarities between the O and $\cdot\text{OH}$ density trends near the liquid surface strengthens our previous assertion that this reduction in density is a product of diminished flow velocity. As O and $\cdot\text{OH}$ are thought to be similarly reactive in the gas phase, a slowing flow rate should manifest as a proportional decrease in density.

3.2. Transport of atomic oxygen and the hydroxyl radical in the liquid phase

Measurements of $\cdot\text{OH}$ and O in the gas phase are critical for understanding the delivery of these reactive species to

plasma-treated liquid. The importance of using gas phase measurements to contextualize those performed in the liquid is amplified by the numerous shortcomings of liquid-phase diagnostics, especially in the presence of atomic O. These include a lack of selectivity when both $\cdot\text{OH}$ and O are present [9, 19], the propensity of atomic oxygen to degrade chemical probes [8, 36], and an absence of aqueous phase reaction rate data for O [37].

Table 1 shows a comparison of OH and O fluxes measured at the liquid interface using gas phase densities obtained by LIF ($\cdot\text{OH}$) and TALIF (O) [27] along with liquid diagnostics for H₂O₂ in DI water, which is mainly formed through OH recombination, and TEMPO, a product of the EPR spin trap TEMP with atomic oxygen [19]. The ratios between He/O₂ and He/H₂O for the O flux to the liquid and TEMPO formation are in very good agreement. Discrepancies of a factor of 4.2 between the ratios of relative OH flux to the liquid and H₂O₂ concentration in the liquid for He/O₂ and He/H₂O can be observed. This is most likely due to the abundance of atomic oxygen in the He/O₂ discharge with consecutive transport into the liquid, as visualized in figure 5.

The solvation of atomic O leads to efficient reactions between O_{aq} and H₂O₂ via the reaction ($k = 1.6 \times 10^9$) [38]:



which reduces the H₂O₂ concentration in He/O₂ plasma-treated water.

Taking a closer look at the H₂O₂ concentrations for both gas admixtures, it has been shown previously that H₂O₂ forms to a large extent in the gas phase for the He/H₂O gas admixture, while it is formed primarily in the liquid for the He/O₂ gas admixture [19]. This has important implications when biological samples are treated as the precursors to form H₂O₂ ($\cdot\text{OH}$, HO₂) are typically more reactive than H₂O₂ itself. One possible pathway of H₂O₂ formation in He/O₂-treated liquid containing organic molecules is the H abstraction by atomic oxygen [19] so that the organic molecules in the liquid become part and may play a crucial role in the liquid phase chemistry. Previous research has shown that H₂O₂ production in DI water compared to a solution of the spin trap DMPO and a TA solution remains the same for He/H₂O, but differs significantly for He/O₂ plasma-treated solutions [19]. An excess H₂O₂ production in the He/O₂ case has also been reported for phenol solutions [8]. It was postulated that O abstracted hydrogen atoms reacted with aqueous O₂ to produce HO₂ radicals ($k = 10^{10} \text{ M}^{-1} \text{ s}^{-1}$) [8, 19]. The HO₂ radicals can subsequently self-react to form H₂O₂ ($k = 10^6 - 10^7 \text{ M}^{-1} \text{ s}^{-1}$) [39] or react with H \cdot to form H₂O₂ ($k = 10^{10} \text{ M}^{-1} \text{ s}^{-1}$) [40].

In order to understand the possible biological implications of O and OH in the aqueous phase, cysteine was used as a model substrate later in this publication. However, given that H abstraction could occur on cysteine from atomic oxygen leading to increases in H₂O₂ concentrations, H₂O₂ measurements were taken for He/O₂ and He/H₂O plasma-treated DI water and cysteine solutions, depicted in figure 6, to elucidate any additional reaction pathways resulting in cysteine modifications. Furthermore, the concentration of H₂O₂ alone

Table 1. Comparison of $\cdot\text{OH}$ and O fluxes measured at a liquid surface using gas phase diagnostics along with concentrations after one minute of plasma treatment of H_2O_2 in DI water (primarily formed through OH self-reaction) and TEMPO, a product of O and the spin-trap TEMP. Very good agreement is observed for the relative O flux and TEMPO formation between the two admixtures, while O_{aq} efficiently reacting with H_2O_2 may explain the low ratio of H_2O_2 compared to the OH flux in the case of the He/ O_2 admixture.

Gas admixture	$\cdot\text{OH}$ LIF (A.U.)	H_2O_2 (μM)	O flux (s^{-1})	TEMPO (μM)
He/ O_2	1.98×10^4	4.9	6.1×10^{15}	413.8
He/ H_2O	2.29×10^5	237.7	4.9×10^{14}	32.78
Ratio	1:11.6	1:48.8	12.6:1	12.5:1

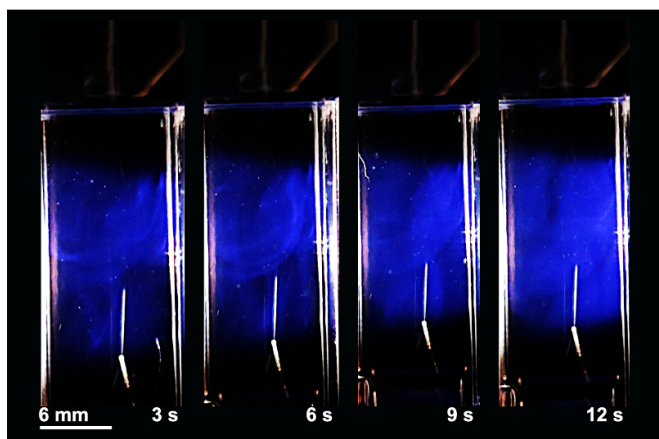


Figure 5. HTA fluorescence shows the transport of atomic oxygen in liquid.

corresponding to the H_2O_2 concentrations produced in a He/ H_2O discharge at each treatment time was investigated to check if H_2O_2 is consumed by cysteine in the liquid. Finally, the pH of the treated cysteine solutions were similar across both admixtures, indicating that the pH did not contribute to the difference in H_2O_2 concentrations.

For 0.5 min and 1 min He/ H_2O treatment, the DI water and mock-treated cysteine solutions show good agreement. For 5 min treatment time, the H_2O_2 concentrations differ significantly (note the axis breaks in figure 6). While this has not been observed for phenol [8] or DMPO and TA solutions [19], it indicates that cysteine indeed consumes H_2O_2 , after an initial reaction with more reactive species had to occur since the H_2O_2 mock treatment does not show a decreased H_2O_2 concentration, which will be discussed in more detail later in this publication. In case of He/ O_2 plasma-treated solutions, the H_2O_2 concentrations are much lower, as expected (note the axis break). Surprisingly, the H_2O_2 concentration is higher in the DI water case and lower for the cysteine solution. This is opposed to what has been observed for phenol [8], and DMPO and TA solutions [19]. For these solutions, H abstraction by O atoms was suggested as potential pathway for H_2O_2 production. It appears that in the case of cysteine, a different reaction pathway has to be considered, which will be discussed in more detail in section 3.3.

3.3. Cysteine modifications after He/ O_2 and He/ H_2O treatment

Cysteine in aqueous solution was treated with the COST-jet operated in He/ O_2 and He/ H_2O . Modifications on the model

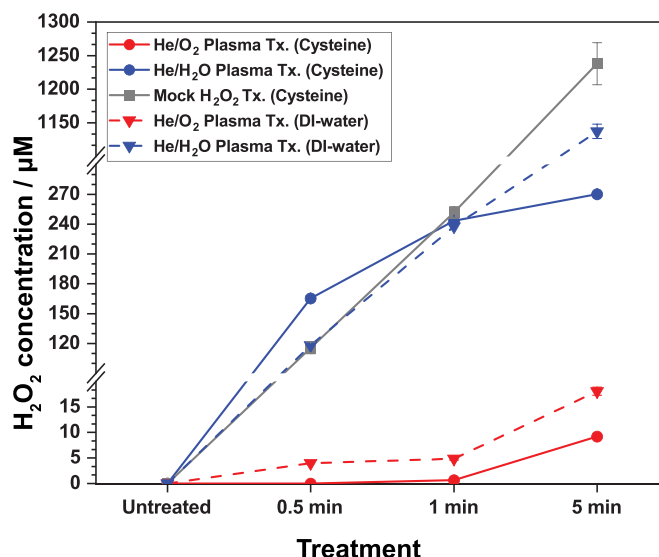


Figure 6. Hydrogen peroxide concentrations for cysteine solutions after He/ O_2 and He/ H_2O treatment compared to mock treatment of cysteine (H_2O_2 was added in the concentrations equivalent to the H_2O_2 concentrations for the He/ H_2O treatment times) and H_2O_2 production in DI water, taken from. Reproduced from [19]. © IOP Publishing Ltd. All rights reserved.

substrate cysteine were investigated by means of FTIR spectroscopy and mass spectrometry. Several common and unique modifications were observed, as described in the following. Figure 7 depicts the structures of the native cysteine together with the most important modifications observed after plasma treatment. As shown in previous work by using MD simulations, one initial reaction is the H-abstraction from the thiol group ($-\text{SH}$) by OH with a probability of 30%, yielding a reactive sulfur [3]. From there, two reactive Cys($-\text{H}$) can combine to form cystine. Another pathway is the addition of OH to the native cysteine with a probability of 50%, yielding Cys-SOH₂ as intermediate. Upon further reaction with OH, O₂, or O₃, the transient cysteine sulfenic acid is formed, followed by the higher oxidation states cysteine sulfinic and sulfonic acid. Note that H_2O_2 was not included in the MD simulations in previous work, as the reactions occur on significantly longer timescales than the 10 ps studied [3]. Atomic oxygen could not be included in the MD simulations due to the lack of available rate constants.

Figure 8 depicts FTIR spectra of cysteine treated in aqueous solution for 1 min with He/ O_2 plasma, He/ H_2O plasma, and H_2O_2 in the same concentration as produced in the He/ H_2O plasma settings after 1 min treatment time. As control, the gas control for He/ O_2 is shown representative for the control

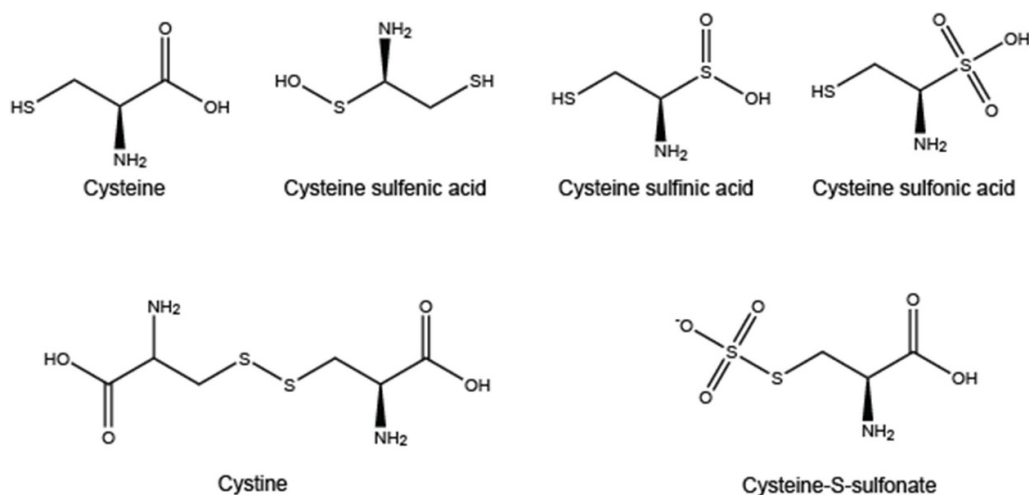


Figure 7. Structures of the unmodified cysteine and the most prominent modifications observed after plasma treatment. Cysteine can oxidize to the intermediates cysteine sulfinic acid and cysteine sulfonic acid, with the last oxidation stage being cysteine sulfonic acid. Once the H-abstraction from the thiol (-SH) group occurred, cysteine can form. Different pathways can lead to cysteine-S-sulfonate formation (see text).

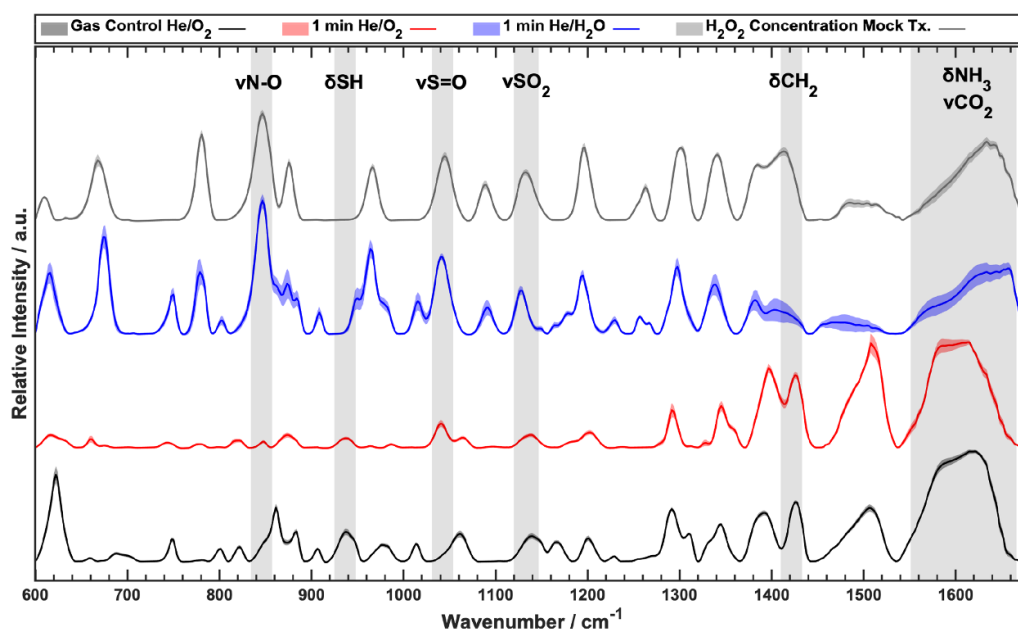


Figure 8. FTIR spectra of cysteine after 1 min treatment with He/O₂, He/H₂O, and H₂O₂ in the same concentration as produced in the He/H₂O plasma settings. As control, the gas control for He/O₂ is shown representative for the control spectra taken. He/O₂ plasma treatment of the cysteine solution leads to a general loss in signal. While the SH bending signal decreases, S=O stretching and SO₂ stretching signals appear. For He/H₂O treated cysteine, the SH bending signal vanishes, S=O stretching and SO₂ stretching signals appear, as well as a distinct N–O stretching.

spectra taken (untreated control, He/O₂ gas control, He/H₂O gas control). As previously reported for the He/O₂ gas admixture in the COST-jet [3], a loss of signal for the thiol group (-SH) in conjunction with an increase of the S=O stretching is observed.

A general impact on the cysteine backbone structure could be observed as well. The signals between 1300 cm⁻¹ and 1650 cm⁻¹ which correspond to the amino, carboxyl, and α-C regions were sharp and well defined in the controls and became less defined after plasma treatment. In case of the He/O₂ treatment, a distinct loss in the -SH bending signal and

a distinct increase of the S=O stretching with a general loss of signal and definition of the bands can be observed. On the other hand, He/H₂O treated samples show several peaks and structures in addition, as well as a larger standard deviation for the treated samples, indicating a variety of modifications occurring upon exposure to the reactive species. Compared to the H₂O₂ mock treatment, where cysteine was exposed to the same concentration of hydrogen peroxide as produced by the He/H₂O plasma treatment after 1 min, the SH bending signal vanishes and the S=O stretching and SO₂ stretching signals appear in a similar manner. The standard deviation in the

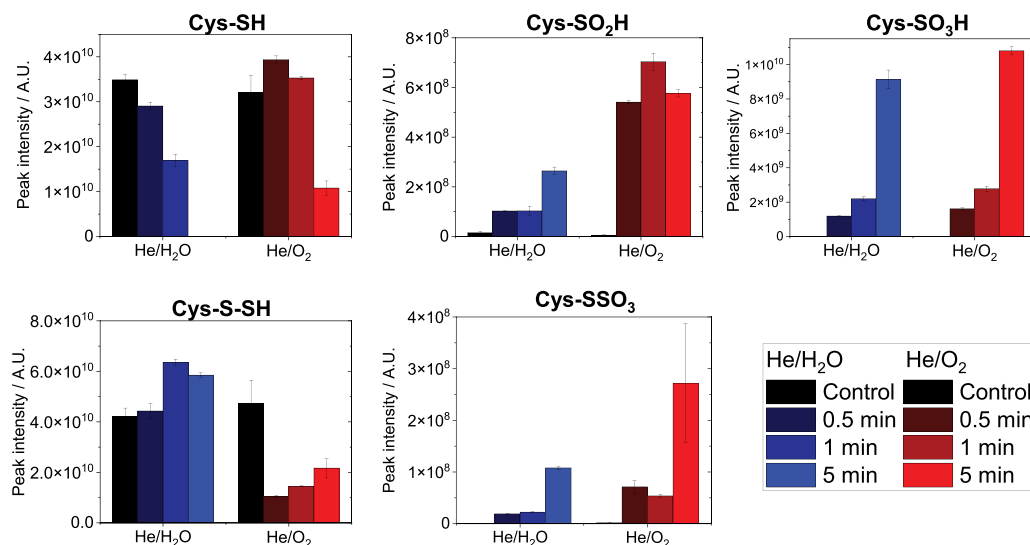


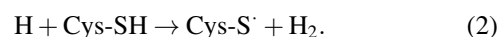
Figure 9. Peak intensities of the most prevalent modifications identified with mass spectrometry after plasma treatment with He/H₂O (blue) and He/O₂ (red) at 0.5, 1, and 5 min. Plotted are from top left to bottom right: native cysteine (RSH), cysteine sulfinic acid (RSO₂), cysteine sulfonic acid (RSO₃), cystine (RSSR), and cysteine-S-sulfonate (RSSO₃).

He/H₂O plasma-treated samples is larger, in particular in the backbone region indicated by the signals between 1300 cm⁻¹ and 1650 cm⁻¹ which correspond to the amino, carboxyl, and α -C regions. At the same time, the rise of the N–O stretching signal at 848 cm⁻¹ and the N=O stretching at 1490 cm⁻¹ may indicate the formation of S-nitrosothiols or oxidation of the amino region [21, 41].

Mass spectrometry (figure 9) revealed that the native cysteine (Cys-SH) disappears completely after 5 min He/H₂O treatment and is still present, if drastically reduced, after 5 min He/O₂ treatment.

The primary modification from He/H₂O treatment is the formation of cystine (Cys-S-S-Cys), whereas He/O₂ treatment results in oxidation to sulfinic (Cys-SO₂H) and sulfonic (Cys-SO₃H) acids. This is supported by the FTIR spectra, which show S=O stretching for He/O₂ plasma treatment. Due to its chemical instability, no traces of sulfenic acid (Cys-SOH) could be detected. Cysteine-S-sulfonate (Cys-S-SO₃H) is produced to a greater extent in the He/O₂ discharge. Wende *et al* reported the production of cysteine-S-sulfonate, sulfate, sulfide in He/O₂ (COST-jet) and Ar/O₂ (kINPen) [7], with a preference for production under the He/O₂ COST-jet conditions. Different pathways can lead to the production of cysteine-S-sulfonate, discussed in more detail in the next section. As mentioned above, the initial reaction is either the H abstraction (30% probability) or OH addition (50% probability) to the thiol moiety of cysteine [3], as observed with MD simulations. The MD simulations did not include H₂O₂ and O. Assuming that the initial reaction indeed is caused by \cdot OH ($k = 1.9 \times 10^{10} \text{ M}^{-1} \text{ s}^{-1}$, almost pH-independent [42]), the consecutive reactions must defer between He/O₂ and He/H₂O conditions. The H abstraction yields a reactive sulfur which can form cystine as observed to a large extent for the He/H₂O case, or be further oxidized to form sulfinic, sulfinic, and ultimately sulfonic acid, the major modifications observed

with He/O₂. An alternative pathway that was not included in MD simulations is the H addition to cysteine, yielding a reactive sulfur radical as well:



There are no rate constants available for this process, thus it is difficult to determine if this process plays a major role in the initiation of the reactions. As a significant amount of H is produced in the He/H₂O discharge and transported into the liquid [18, 20] it may contribute to the production of cystine in the He/H₂O case. To further elucidate the reaction pathways, cysteine was treated in heavy water H₂¹⁸O to determine the origin of species responsible for the observed modifications.

3.4. The origin of species

Heavy water H₂¹⁸O was used for cysteine solutions to determine the origin of species responsible for plasma-induced modifications on cysteine. The graph shows ratios of oxidative modifications occurring on cysteine after 0.5 min, 1 min, and 5 min treatment with He/H₂O (top) or He/O₂ (bottom), normalized to 1 for the total oxygen contribution for each molecule. The incorporation of liquid-derived ¹⁸O into Cys-SO₂H, Cys-SO₃H and Cys-S-SO₃H indicates that reactive species are produced in the liquid phase. It is apparent that Cys-SO₂H and Cys-SO₃H are produced to a greater extent by ROS created in the gas phase, while Cys-S-SO₃H shows the incorporation of liquid-derived oxygen for both gas admixtures. This is in good agreement with a study performed by Wende *et al* [7] for the kinpen in comparison to a He/O₂ jet treatment.

In the case of 1 min. He/O₂ treatment, 72.4% and 65.7% of the in Cys-SO₂H and Cys-SO₃H incorporated oxygen originates in the gas phase. Our results indicate a slightly higher

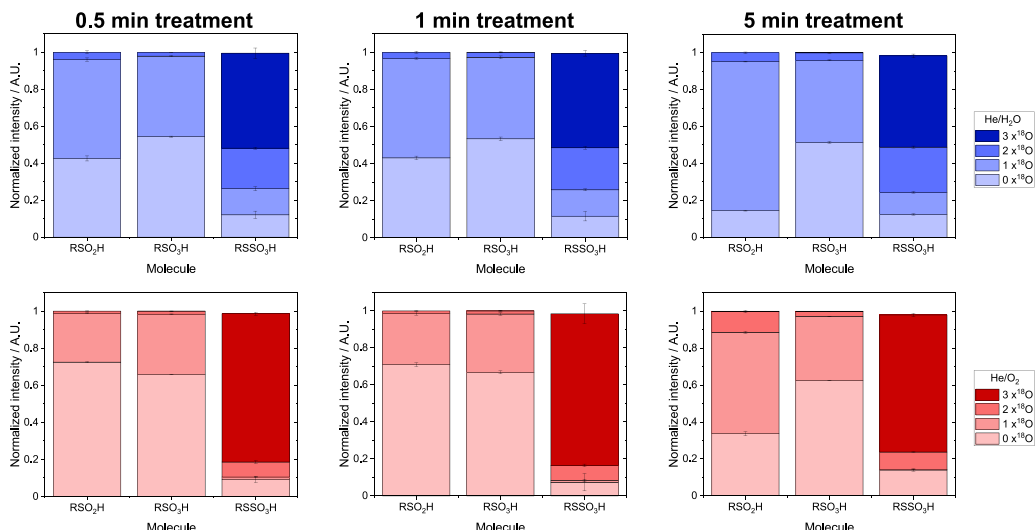
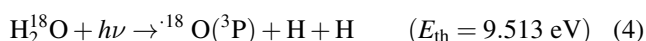
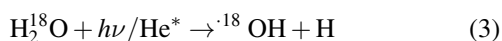


Figure 10. Heavy oxygen ^{18}O contribution to oxidation states of cysteine during He/ H_2O (top, blue) and He/ O_2 (bottom, red) plasma treatment.

percentage of gas phase oxygen compared to Wende *et al* [7] which could be explained by the difference in oxygen admixture in the feed gas (0.6% O_2 , which has been shown to produce the highest concentration of atomic oxygen [43] compared to 1% O_2 in [7]), thus a higher flux of atomic oxygen generated in the gas phase is entering the liquid. For 1 min. He/ H_2O , only 42% and 54% of the in Cys- SO_2H and Cys- SO_3H incorporated oxygen originates in the gas phase, thus the ratio of liquid phase and gas phase oxygen is closer to 1:1. For the 5 min treatment time, 33% and 62% of the in Cys- SO_2H and Cys- SO_3H incorporated oxygen originates in the gas phase for He/ O_2 and only 14% and 52% in the case of He/ H_2O . After 5 min treatment time, the ratios of ^{16}O to ^{18}O for Cys- SO_3H remain relatively constant for both gas admixtures while the contributions of ^{18}O rise significantly in Cys- SO_2H for both gas admixtures (He/ H_2O : 14% originate in gas phase, He/ O_2 : 33% originate in gas phase).

Cysteine-S-sulfonate shows a high levels of ^{18}O incorporation for both gas admixtures, with the ratios of contribution being relatively similar for all time points investigated. To compare the two gas admixtures in more detail, at 1 min treatment time Cys-S- SO_3H in the He/ H_2O case incorporated 11% gaseous ^{16}O , 14% were detected with one ^{18}O , 22% with two ^{18}O , and 50% with three ^{18}O . For He/ O_2 , only 7% gaseous ^{16}O were detected (compared to 9% in [7]), 10% were detected with one ^{18}O , 8% with two ^{18}O , and 82% with three ^{18}O . There are several pathways to create Cys-S- SO_3H , as described and discussed in detail by Wende *et al* [7]. Wende *et al* concluded that Cys-S- SO_3H is produced in the bulk liquid by $\cdot\text{OH}$ generated from the liquid following reaction (5), see below.

There are several possible pathways for the production of ^{18}O in heavy water prior to further reaction with cysteine:



Reaction (3) describes water cleavage by the impact of photons or metastables. He metastables are unlikely to reach the water interface 4 mm from the active plasma region when molecular gas admixtures are used, as He metastables are easily quenched [44]. As water absorbs radiation below 200 nm [45], VUV photons would be required for this reaction. Hefny *et al* reported that the addition of just 100 ppm of any molecular gas quenches the He excimer emission and concluded that the effect of energetic photons is negligible [8]. Radiances of atomic oxygen lines (115 nm and 130 nm) have been measured at a distance of 4 mm in He/ O_2 (0.6%) in controlled helium atmosphere [46]. The $10 \mu\text{W mm}^{-2} \text{sr}^{-1}$ reported present thus an upper limit for our open air effluent in contact with a liquid interface. The three-body dissociation reaction (4) has a threshold energy of 9.513 eV which corresponds to the atomic oxygen line emission at 130.2 nm (9.5 eV). Further atomic oxygen lines (94.9 nm (13 eV), 98.9 nm (12.5 eV), 115.2 nm (10.72 eV)) as well as atomic hydrogen lines were recently reported for the COST-jet for He/ O_2 in controlled helium atmosphere by Golda *et al* [47], again providing an upper limit due to the open atmosphere and the liquid interface used in this study. Nonetheless, liquid water has a local energy absorption cross section maximum at 9.8 eV ($\sigma = 8 \times 10^{-18} \text{cm}^2/\text{molecules}$), increasing to about $\sigma = 20 \times 10^{-18} \text{cm}^2/\text{molecules}$ for 13 eV [48]. Although the number of VUV photons reaching the liquid interface is most likely low under the experimental conditions used, it may be enough to initiate reactions in the water by hydrolysis. Reaction (5) has been suggested as another potential reactant for water cleavage [9, 49], but in conditions with the highest atomic O density (He/ O_2 compared to He/ H_2O), the lowest inclusion of ^{18}O was observed. This aligns well with the results presented in [7]. Protonated water clusters $\text{H}^+(\text{H}_2\text{O})_n$ have been shown to reach distances of up to 10 mm, with a preference for heavier clusters ($n = 6-8$) further away from

the active plasma [50]. Ions are recombining quickly in the effluent and the expected densities at 4 mm distance are low [50] but their impact can not be ruled out. Another possibility would be that gaseous ^{16}OH enters the liquid and undergoes H transfer with H_2^{18}O [51, 52], so that gas phase ^{16}OH would be able to create liquid phase $^{18}\text{OH}_{\text{aq}}$.

Once ^{18}OH or ^{18}O has been created, they can modify cysteine directly or undergo a variety of liquid reactions forming other reactive species, e.g. $\text{H}_2^{18}\text{O}^{16}\text{O}$, $\text{H}^{18}\text{O}^{16}\text{O}$, thus transporting and accumulating ^{18}O in reactive species.

4. Discussion

The data taken together depict the outcome of species generated in the gas in the presence of a liquid interface, their delivery into the liquid phase, reactions with molecules in the liquid and ability to modify a model substrate. The plasma-generated ^{16}OH from He/ H_2O was shown to mainly form H_2O_2 in the gas phase prior to solvating in the liquid phase, whereas the He/ O_2 admixture generated O which crosses the liquid interface and requires a substrate in the liquid for H_2O_2 production through H abstraction [9, 19]. Regardless of where the H_2O_2 is produced, an initiating reaction from H, O or OH is required for the modification of cysteine [3], as evidenced by the unaltered mock treatment hydrogen peroxide concentration shown in figure 6. Since H, O and OH are required in both the liquid and gas phases for initiation, modification, and production reactions, understanding their source and sink reactions as well as their flux between phases is needed to ensure sufficient species concentrations for all reactions. Taken together with previous literature for the COST-jet, this study provides a framework for a more targeted approach for the delivery of plasma-generated species.

Hydrogen peroxide and OH are physiologically relevant ROS, whereas atomic oxygen is unknown to biological systems. It is thus not surprising that the cysteine products after He/ H_2O treatment include the reversible modifications cystine (Cys-S-S-Cys) and cysteine-S-sulfonate (Cys-S-SO₃) [23, 53], while the He/ O_2 -exposed samples show more distinct sulfur-oxidations, most of which are irreversible modifications (sulfinic acid, sulfonic acid) [23]. H_2O_2 can directly oxidize cysteine, yielding sulfinic acid [23]. Sulfinic acid can then be stabilized by forming a disulfide or sulfenamide state to protect against irreversible overoxidation. In the presence of excess H_2O_2 (or potentially other ROS), sulfinic acid can be further oxidized to sulfinic (Cys-SO₂H) and sulfonic acid (Cys-SO₃H). The disulfide form cystine can be further oxidized by H_2O_2 (and potentially other ROS) to form cysteine-S-sulfonate, which can also be formed by the attack of $^{\cdot}\text{SH}$ -derived species such as sulfite (SO_3^{2-}) on cysteine, cystine, or the thiyl radical (Cys-S $^{\cdot}$) [7, 54]. The transfer of atomic O into the liquid phase was first shown by Benedikt *et al* [9]. In the presence of ring structures, atomic O was shown to abstract H and produce secondary compounds like H_2O_2 [9, 19]. Without this structure, atomic oxygen is able to interact directly with or indirectly through other molecules to effectively oxidize cysteine outside of H_2O_2 . While little

H_2O_2 is produced, the modifications shown by mass spectrometry indicate that atomic oxygen itself may be able to initiate and then oxidize cysteine to irreversible levels without producing relatively comparable levels of reversible modifications. In order for OH dominated chemistry to oxidize cysteine to these levels, large quantities of H_2O_2 must be produced to overoxidize sulfinic acid.

Another difference between the O and OH dominated chemistry can be seen in the backbone modifications of cysteine, as seen in figure 8. The bands corresponding to the backbone (between 1300 cm^{-1} and 1650 cm^{-1} , corresponding to the amino, carboxyl, and α -C regions) were modified to a greater extent in He/ H_2O and in the H_2O_2 control. Comparing the H_2O_2 control with the He/ H_2O plasma treatment, the loss in signal as well as the standard deviation is greater for the plasma-treated samples, indicating a variety of modifications occur. Under He/ O_2 conditions, the backbone seems only slightly modified. It is believed that oxidants like H_2O_2 usually attack amino acid side chains and not the backbone [55]. Strong oxidizing agents may oxidize the amino acid backbone as well, resulting in backbone fragmentation. It has been observed in biological systems that subsequent formation of the peroxy radical in the presence of O_2 is necessary for backbone cleavage [56]. In the He/ H_2O treatment case, hydroperoxyl radicals are generated in the gas phase by reactions of H_2O_2 with H or OH, of OH and O_3 , or H and O_2 (with He as third body) [10] and transported efficiently into the liquid (with a Henry constant of 1.68×10^4 [57]). Furthermore, reactions in the liquid phase, e.g.



can produce the hydroperoxyl radical. The production of the hydroperoxyl radical is very efficient in the He/ O_2 case with the H_2O_2 concentration being the rate-limiting factor. In case of the He/ H_2O case, the rate constant is two orders of magnitude lower but there is an abundance of H_2O_2 and OH present in the liquid. In addition, as mentioned above, HO_2^{\cdot} is produced in the gas phase and transported into the liquid. The backbone modifications observed could thus be explained by the production of hydroperoxyl radicals which are able to attack the amino acid backbone, leading eventually to backbone fragmentation.

The H_2O_2 measurements give further insights into the reaction pathways. In case of the He/ H_2O plasma treatment, the H_2O_2 concentrations are comparable in DI water and cysteine solutions for 1 min treatment time and significantly lower in the cysteine solution after 5 min treatment time. In previous studies, TA and DMPO solutions did not alter the H_2O_2 concentrations in He/ H_2O treated solutions [19]. As most of the hydrogen peroxide is already generated in the gas phase, this indicates that cysteine reduces H_2O_2 . Compared to the H_2O_2 mock treatment, where no reduction of H_2O_2 was observed, it indicates that an initial reaction has to be performed with a more reactive species generated in the plasma or the liquid,

e.g. O, OH, or H. While it has been observed for ring structures [9, 19] that H₂O₂ is produced in He/O₂ plasma-treated solutions in the presence of organic matter by H abstraction, in case of cysteine solutions the H₂O₂ was observed to be higher in the DI water case, indicating that no additional H₂O₂ is produced by H abstraction. In fact, the H₂O₂ concentration is lower when cysteine is present, implying that cysteine reduces H₂O₂ or reacts with precursors before they can form H₂O₂. This confirms the previously performed MD simulations [3], in which it was predicted that H abstraction is not the major initial step for cysteine modifications. Instead, the addition of OH was found to be the more prevalent initial modification. There is no data available if O would add in a similar manner to cysteine. Since ·OH can be produced in He/O₂-treated liquids via reaction (1) as well, it is not possible to identify the initial reaction with the data available.

The observed modifications to cysteine show that both admixtures effectively alter the structure of the model substrate. For biological applications of non-thermal plasma, the resulting effects from treatment will depend on how the structures are modified and if these modifications are reversible. Typically, plasma treatments degrade proteins and chemical probes [9, 19, 59], however Krewing *et al* could show reversible activation of oxidized cysteine residues [59]. In combination with the results presented in this paper, this suggests that the resultant plasma-induced modifications, whether it is activation or degradation, could be managed at the plasma parameter input level. An efficient oxidation method for a biological target may be desired, however the overoxidation of these targets may be outside of the preferred outcome and occur on time scales faster than those of biological responses. For these reasons, a tailored approach for the delivery of plasma-generated species in biological applications must consider the generation of these species in the gas and liquid phase, the flux of the species across the gas–liquid interface, and the resulting chemistry and modification to the biological target.

5. Conclusions

He/O₂ (0.6%) and He/H₂O (0.25%) gas admixtures in the COST atmospheric pressure plasma jet were used to study the generation and transport of O and ·OH from the gas phase to the liquid to the biological model target cysteine. The COST-jet is an efficient source of O in He/O₂ gas admixtures and an efficient source of OH/H₂O₂ in the He/H₂O gas admixture. By using heavy water (H₂¹⁸O) and mass spectrometry, the impact of liquid-derived reactive species was studied. The liquid chemistry in He/H₂O discharges appears more complex as the incorporated ¹⁸O was found to be higher in He/H₂O treated cysteine. Taken together with FTIR analysis of cysteine after treatment, it can be concluded that an initial reaction with plasma-derived OH, O, or H must take place before further reactions follow. The reaction pathways differ significantly for He/O₂ and He/H₂O; while He/O₂ mainly targets the sulfur moiety of cysteine for oxidation up to irreversible oxidation states, He/H₂O treatment leads preferentially to reversible oxidation products. This highlights that atomic oxygen is

unknown to biological systems, while H₂O₂ and ·OH are physiologically relevant ROS. The more O or OH/H₂O₂ dominated ROS produced by the two gas admixtures studied offers the possibility to select species for target modification. By tailoring where the species are produced and how many initiating reaction molecules are required will determine the approach for biological targets or agricultural applications.

Data availability statement

The data that support the findings of this study are available upon reasonable request from the authors.

Acknowledgments

This material is based partly upon work supported by the U.S. Department of Energy, Office of Science, Office of Fusion Energy Sciences Opportunities in Frontier Plasma Science program under Award Number DE-SC-0021329. Part of this research used resources of the Sandia National Laboratory, which is a DOE Office of Science User Facility. The authors gratefully acknowledge Ed Barnat's support for the TALIF and LIF experiments at Sandia National Laboratory and thank for fruitful discussions. This material is partly based upon work supported by the U.S. Department of Energy, Office of Science, Office of Workforce Development for Teachers and Scientists, Office of Science Graduate Student Research (SCGSR) program. The SCGSR program is administered by the Oak Ridge Institute for Science and Education (ORISE) for the DOE. ORISE is managed by ORAU under Contract Number DE-SC0014664. All opinions expressed in this paper are the author's and do not necessarily reflect the policies and views of DOE, ORAU, or ORISE. This work was performed in part by the Molecular Education, Technology and Research Innovation Center (METRIC) at NC State University, which is supported by the State of North Carolina.

ORCID iDs

Katharina Stapelmann  <https://orcid.org/0000-0002-2116-2661>

Maria Herrera Quesada  <https://orcid.org/0000-0002-8623-550X>

Pietro J Ranieri  <https://orcid.org/0000-0002-3644-8558>

References

- [1] Bekešchus S *et al* 2017 Oxygen atoms are critical in rendering THP-1 leukaemia cells susceptible to cold physical plasma-induced apoptosis *Sci. Rep.* **7** 1–12
- [2] Lin A *et al* 2019 Non-Thermal plasma as a unique delivery system of short-lived reactive oxygen and nitrogen species for immunogenic cell death in melanoma cells *Adv. Sci.* **6** 1802062
- [3] Lackmann J W *et al* 2018 Chemical fingerprints of cold physical plasmas—an experimental and computational study using cysteine as tracer compound *Sci. Rep.* **8** 7736

- [4] Klinkhammer C *et al* 2017 Elucidation of plasma-induced chemical modifications on glutathione and glutathione disulphide *Sci. Rep.* **7** 1–11
- [5] Bruno G, Heusler T, Lackmann J W, Von Woedtke T, Weltmann K D and Wende K 2019 Cold physical plasma-induced oxidation of cysteine yields reactive sulfur species (RSS) *Clin. Plasma Med.* **14** 100083
- [6] Lackmann J W *et al* 2019 Nitrosylation vs. oxidation-how to modulate cold physical plasmas for biological applications *PLoS One* **14** e0216606
- [7] Wende K *et al* 2020 On a heavy path–determining cold plasma-derived short-lived species chemistry using isotopic labelling *RSC Adv.* **10** 11598–607
- [8] Hefny M M, Pattyn C, Lukes P and Benedikt J 2016 Atmospheric plasma generates oxygen atoms as oxidizing species in aqueous solutions *J. Phys. D: Appl. Phys.* **49** 404002
- [9] Benedikt J *et al* 2018 The fate of plasma-generated oxygen atoms in aqueous solutions: non-equilibrium atmospheric pressure plasmas as an efficient source of atomic O (aq) *Phys. Chem. Chem. Phys.* **20** 12037–42
- [10] Schröter S *et al* 2018 Chemical kinetics in an atmospheric pressure helium plasma containing humidity *Phys. Chem. Chem. Phys.* **20** 24263–86
- [11] Golda J *et al* 2016 Concepts and characteristics of the 'COST Reference Microplasma Jet *J. Phys. D: Appl. Phys.* **49** 84003
- [12] Golda J *et al* 2019 Dissipated electrical power and electron density in an RF atmospheric pressure helium plasma jet *Plasma Sources Sci. Technol.* **28** 095023
- [13] Ellerweg D, Von Keudell A and Unexpected B J 2012 O and O₃ production in the effluent of He/O₂ microplasma jets emanating into ambient air *Plasma Sources Sci. Technol.* **21** 034019
- [14] Große-Kreul S *et al* 2015 Mass spectrometry of atmospheric pressure plasmas *Plasma Sources Sci. Technol.* **24** 044008
- [15] Benedikt J *et al* 2016 Absolute OH and O radical densities in effluent of a He/H₂O micro-scaled atmospheric pressure plasma jet *Plasma Sources Sci. Technol.* **25** 045013
- [16] Knake N, Niemi K and Reuter S, Schulz-von der Gathen V and Winter J 2008 Absolute atomic oxygen density profiles in the discharge core of a microscale atmospheric pressure plasma jet *Appl. Phys. Lett.* **93** 131503
- [17] Korolov I *et al* 2021 Atomic oxygen generation in atmospheric pressure RF plasma jets driven by tailored voltage waveforms in mixtures of He and O₂ *J. Phys. D: Appl. Phys.* **54** 125203
- [18] Schröter S *et al* 2020 The formation of atomic oxygen and hydrogen in atmospheric pressure plasmas containing humidity: picosecond two-photon absorption laser induced fluorescence and numerical simulations *Plasma Sources Sci. Technol.* **29** 105001
- [19] Myers B *et al* 2021; Measuring plasma-generated •OH and O atoms in liquid using EPR spectroscopy and the non-selectivity of the HTA assay *J. Phys. D: Appl. Phys.* **54** 145202
- [20] Gorbanev Y *et al* 2018 Combining experimental and modelling approaches to study the sources of reactive species induced in water by the COST RF plasma jet *Phys. Chem. Chem. Phys.* **20** 2797–808
- [21] Kogelheide F *et al* 2016 FTIR spectroscopy of cysteine as a ready-to-use method for the investigation of plasma-induced chemical modifications of macromolecules *J. Phys. D: Appl. Phys.* **49** 084004
- [22] Offerhaus B *et al* 2017 Spatially resolved measurements of the physical plasma parameters and the chemical modifications in a twin surface dielectric barrier discharge for gas flow purification *Plasma Process. Polym.* **14** 1600255
- [23] Paulsen C E and Carroll K S 2013 Cysteine-mediated redox signaling: chemistry, biology and tools for discovery *Chem. Rev.* **113** 4633–79
- [24] Trivedi M V, Laurence J S and Siahaan T J 2009 The role of thiols and disulfides on protein stability *Curr. Protein Peptide Sci.* **10** 614–25
- [25] Randall L O 1946 Reaction of thiol compounds with peroxidase and hydrogen peroxide *J. Biolo. Chem.* **164** 521–7
- [26] Gould N, Doulias P T, Tenopoulou M, Raju K and Ischiropoulos H 2013 Regulation of protein function and signaling by reversible cysteine S-nitrosylation *J. Biol. Chem.* **288** 26473–9
- [27] Myers B, Barnat E and Stapelmann K 2021 Atomic oxygen density determination in the effluent of the COST Reference Source using in situ effective lifetime measurements in the presence of a liquid interface *J. Phys. D: Appl. Phys.* (submitted)
- [28] Luque J and Crosley D R 1998 Transition probabilities in the A²Σ⁺ – X²Π_i electronic system of OH *J. Chem. Phys.* **109** 439–48
- [29] Niemi K, von der Gathen V S and Döbele H F 2005 Absolute atomic oxygen density measurements by two-photon absorption laser-induced fluorescence spectroscopy in an RF-excited atmospheric pressure plasma jet *Plasma Sources Sci. Technol.* **14** 375–86
- [30] Yonemori S, Nakagawa Y, Ono R and Oda T 2012 Measurement of OH density and air-helium mixture ratio in an atmospheric-pressure helium plasma jet *J. Phys. D: Appl. Phys.* **45** 225202
- [31] Tamura M *et al* 1998 Collisional quenching of CH(A), OH(A) and NO(A) in low pressure hydrocarbon flames *Combust. Flame* **114** 502–14
- [32] Williams L R and Crosley D R 1996 Collisional vibrational energy transfer of OH (A-2Σ⁺, v' = 1) *J. Chem. Phys.* **104** 6507–14
- [33] Adams K J *et al* 2020 Skyline for small molecules: a unifying software package for quantitative metabolomics *J. Proteome Res.* **19** 1447–58
- [34] Gorbanev Y, O'Connell D and Non-Thermal C V 2016 Plasma in contact with water: the origin of species *Chem. Eur. J.* **22** 3496–505
- [35] Hartlieb A T, Markus D, Kreutner W and Kohse-Höinghaus K 1997 Measurement of vibrational energy transfer of OH(A²Σ⁺, (ν' = 1 → 0) in low-pressure flames *Appl. Phys. B* **65** 81–91
- [36] Gorbanev Y, Stehling N, O'Connell D and Chechik V 2016 Reactions of nitroxide radicals in aqueous solutions exposed to non-thermal plasma: limitations of spin trapping of the plasma induced species *Plasma Sources Sci. Technol.* **25** 055017
- [37] of Standards NI, (NIST) T. NDRL/NIST Solution Kinetics Database 2002 (available at: <https://kinetics.nist.gov/solution/>)
- [38] Sauer J M C, Brown W G and Hart E J 1984 Oxygen (3P) atom formation by the photolysis of hydrogen peroxide in alkaline aqueous solutions *J. Phys. Chem.* **88** 1398–400
- [39] De Grey A D 2002 HO₂•: the forgotten radical *DNA Cell Biol.* **21** 251–7
- [40] Thomas J 1963 The rate constants for H atom reactions in aqueous solutions 1 *J. Phys. Chem.* **67** 2593–5
- [41] Larkin P 2017 *Infrared and Raman Spectroscopy: Principles and Spectral Interpretation* (Amsterdam: Elsevier)
- [42] Hoffman M Z and Hayon E 1973 Pulse radiolysis study of sulfhydryl compounds in aqueous solution *J. Phys. Chem.* **77** 990–6
- [43] Ellerweg D, Benedikt J, von Keudell A, Knake N and Schulz-von der Gathen V 2010 Characterization of the effluent of a He/O₂ microscale atmospheric pressure plasma

- jet by quantitative molecular beam mass spectrometry *New J. Phys.* **12** 013021
- [44] Winter J, Sousa J S, Sadeghi N, Schmidt-Bleker A, Reuter S and Puech V 2015 The spatio-temporal distribution of He (23S1) metastable atoms in a MHz-driven helium plasma jet is influenced by the oxygen/nitrogen ratio of the surrounding atmosphere *Plasma Sources Sci. Technol.* **24** 025015
- [45] Ryason P 1978 Hydrogen from the solar photolysis of water *Energy Sources* **4** 1–22
- [46] Schneider S *et al* 2012 The role of VUV radiation in the inactivation of bacteria with an atmospheric pressure plasma jet *Plasma Process. Polym.* **9** 561–8
- [47] Golda J, Biskup B, Layes V, Winzer T and Benedikt J 2020 Vacuum ultraviolet spectroscopy of cold atmospheric pressure plasma jets *Plasma Process. Polym.* **17** 1900216
- [48] Kerr G, Hamm R, Williams M, Birkhoff R and Painter L 1972 Optical and dielectric properties of water in the vacuum ultraviolet *Phys. Rev. A* **5** 2523
- [49] Quiller R, Baker T, Deng X, Colling M, Min B K and Friend C 2008 Transient hydroxyl formation from water on oxygen-covered Au (111) *J. Chem. Phys.* **129** 064702
- [50] Willems G, Benedikt J and Von Keudell A 2017 Absolutely calibrated mass spectrometry measurement of reactive and stable plasma chemistry products in the effluent of a He/H₂O atmospheric plasma *J. Phys. D: Appl. Phys.* **50** 335204
- [51] Codorniu-Hernández E and Kusalik P G 2011 Insights into the solvation and mobility of the hydroxyl radical in aqueous solution *J. Chem. Theory Comput.* **7** 3725–32
- [52] Codorniu-Hernández E and Kusalik P G 2012 Mobility mechanism of hydroxyl radicals in aqueous solution via hydrogen transfer *J. Am. Chem. Soc.* **134** 532–8
- [53] Garcia-Santamarina S, Boronat S and Hidalgo E 2014 Reversible cysteine oxidation in hydrogen peroxide sensing and signal transduction *Biochemistry* **53** 2560–80
- [54] Luo D, Smith S W and Anderson B D 2005 Kinetics and mechanism of the reaction of cysteine and hydrogen peroxide in aqueous solution *J. Pharm. Sci.* **94** 304–16
- [55] Finnegan M, Linley E, Denyer S P, McDonnell G, Simons C and Maillard J Y 2010 Mode of action of hydrogen peroxide and other oxidizing agents: differences between liquid and gas forms *J. Antimicrob. Chemother.* **65** 2108–15
- [56] Walkup L and Kogoma T 1989 *Escherichia coli* proteins inducible by oxidative stress mediated by the superoxide radical *J. Bacteriol.* **171** 1476–84
- [57] Sander R 2015 Compilation of Henry's law constants (version 4.0) for water as solvent *Atmo. Chem. Phys.* **15** 4399–981
- [58] Destailhats H, Colussi A, Joseph J M and Hoffmann M R 2000 Synergistic effects of sonolysis combined with ozonolysis for the oxidation of azobenzene and methyl orange *J. Phys. Chem. A* **104** 8930–5
- [59] Krewing M *et al* 2019 The molecular chaperone Hsp33 is activated by atmospheric-pressure plasma protecting proteins from aggregation *J. R. Soc. Interface* **16** 20180966